Letter

# Magnetization reversal across multiple serial barriers in a single Fe₃O₄ nanoparticle

Sagar Paul [1], Ganesh Kotagiri [1], Rini Ganguly [2], Annapoorni Subramanian [3], Hervé Courtois [2], Clemens B. Winkelmann [2], and Anjan K. Gupta [1]

[1] *Department of Physics, Indian Institute of Technology Kanpur, Kanpur 208016, India*
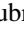[2] *Université Grenoble Alpes, CNRS, Grenoble INP, Institut Néel, 38000 Grenoble, France*
[3] *University of Delhi, Delhi 110021, India*

The depinning of nanoscale magnetic textures, such as domain walls, vortices, and skyrmions, is of paramount importance for magnetic storage and information processing. We measure the time-resolved magnetic switching statistics of an individual, non-single-domain Fe₃O₄ nanoparticle using a micrometer-scale superconducting quantum interference device. A strong narrowing of the waiting-time distributions before reaching the final state is observed as compared to the exponential distribution expected for a single barrier. A model consisting of multiple barriers in series is proposed and used to understand the narrow waiting-time distributions and their evolution with magnetic field. The number of barriers is found to reduce as the thermodynamic switching field is approached and eventually, very close to it, an exponential distribution, resulting from a single barrier, is observed.

DOI: 10.1103/PhysRevB.105.L180410

Ferromagnetic nanostructures display intriguing physics and applications in wide areas, including digital memory [1,2], information processing [3–5], and biomedicine [6]. In the smallest ferromagnetic structures, exhibiting a single magnetic domain, the magnetization reversal occurs through a coherent rotation described by the Stoner-Wohlfarth model [7,8]. In such systems, the switching-time distributions, close to the switching field, are well described by a single exponential with a characteristic time $\tau$. The temperature dependence of $\tau$ is well described by the Néel-Brown model [9–12], based on thermal activation, at high temperatures, and quantum tunneling at low temperatures [13,14]. With increasing size of the nanostructures, the magnetization reversals occur principally through a curling mode involving the inhomogeneous rotation of spins or through the propagation and annihilation of a vortex or a domain wall. In a nanowire, the reversal occurs through vortex-pair nucleation and annihilation and the switching-time distributions show a stretched-exponential decay, with wide switching-field histograms. This is attributed to the presence of many parallel minimum energy pathways (MEPs), with different energy barriers, for the vortex.

In a single nanoparticle, from micromagnetic simulations based on a finite-element solution of the Landau-Lifshitz-Gilbert equation, it is expected that the reversal occurs via the following main steps [15]. When a threshold applied magnetic field is reached, a curling mode or a vortex nucleates at the nanoparticle surface, a process during which only a fraction of the total spins undergo reversal. As the field is further increased, this vortex or curling mode traverses through the nanoparticle volume, by following one of several possible paths. Eventually, at the annihilation field, the magnetization reversal completes, barring some surface spins, as the vortex annihilates. This reversal process can be inferred to some

extent by an analysis of the magnetization cycle. Nevertheless, understanding the mechanisms at stake during the vortex traversal of the nanoparticle requires more information.

In this Letter, we present switching-field and switching-time histograms of single Fe₃O₄ nanoparticles. Both distributions are found to be much narrower than an exponential distribution, and thus too deterministic to be described by a magnetization reversal across a single energy barrier. To understand the measured switching-time histograms, a model involving multiple barriers in series is proposed which leads to a probability distribution which is a convolution of several exponential distributions. In the experiments, the number of serial barriers is found to reduce as the switching field is approached.

Micron or nanometer scale superconducting quantum interference devices ($\mu$- or nano-SQUIDs) have been the most successful probes to date for magnetization reversal studies on individual magnetic nanoparticles [8,14,16] and nanowires [13,17,18] by direct coupling to the SQUID loop. Here, we study the magnetism of individual nanostructures using Nb $\mu$-SQUIDs working in a nonhysteretic mode obtained by an external shunt. An optimized external shunt having both inductance and resistance was found to eliminate thermal hysteresis [19,20] in the current-voltage characteristics of $\mu$-SQUIDs [21,22]. The Nb $\mu$-SQUIDs were fabricated from a 20-nm-thick Nb film using e-beam lithography as described in an earlier work [22] together with the details of the measurement setup including a three-dimensional (3D) vector magnet and its successful use on permalloy nanoneedles. The sensitivity was further improved by using a commercial low-temperature SQUID-array amplifier.

All magnetic measurements in this work were performed with the external field aligned in the $\mu$-SQUID plane, using a
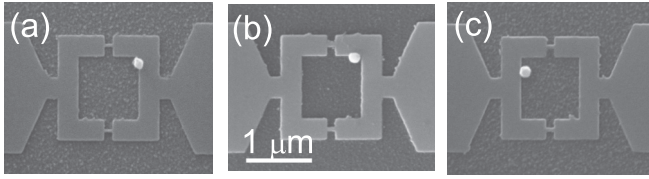
FIG. 1. Scanning electron micrograph of the $\mu$-SQUID with a single $Fe_3O_4$ nanoparticle $F$#1–3 shown in (a)–(c) respectively.



FIG. 2. (a) Measured $M$-$H$ loops of the $Fe_3O_4$ nanoparticle $F$#1 for a field at an in-plane angle $\theta = -45°$ and at $T = 4.0$ K. The loop has two major jumps (marked by arrows) in each field sweep direction due to vortex nucleation and annihilation. The inset of (a) shows the switching-field histograms at the vortex annihilation at positive field. (b) Measured $M$-$H$ loops for the $Fe_3O_4$ nanoparticle $F$#2 (at $T = 4.2$ K, $\theta = 0°$) exhibiting two parallel paths marked by red and black arrows.

3D vector magnet. Switching-field histograms were obtained by repeated ramping of the field at a fixed angle $\theta$, from a negative saturation field and at a specific rate. The applied field $H_{sw}$ at which the sharp jump occurs, due to vortex or domain wall or curling mode annihilation, is recorded in each repetition. Waiting-time histograms were obtained by ramping the field up from a negative saturation field to a positive waiting field $H_w$, just below $H_{sw}$, and noting the time until switching, after arriving at $H_w$.

We present the switching statistics of three $Fe_3O_4$ nanoparticles, namely $F$#1–3 and as shown in Fig. 1, of size $\sim$150 $\pm$ 20 nm and a permalloy nanowire, namely $N$#1, of 2 $\mu$m length, 80 nm width, and 100 nm thickness. The magnetite ($Fe_3O_4$) nanoparticles were synthesized using a simple polyol method [23]. Room-temperature hysteresis measurements in a vibrating sample magnetometer (VSM) were performed on a bulk powder form. These indicate a soft ferromagnetic nature with coercivity $H_c = 235$ Oe and saturation magnetization $M_s = 67.8$ emu/g. The former indicates a nonsuperparamagnetic character while the $M_s$ being smaller than the bulk value of 92 emu/g shows a size smaller than the bulk. A substrate having several $\mu$-SQUIDs was dipped for a few seconds in ethanol with dispersed $Fe_3O_4$ magnetic nanoparticles (MNPs) kept in a sonication bath. The substrate was then immediately placed on a permanent magnet for a fraction of a second to avoid the agglomeration of particles. Repeating this process a number of times yields few devices with single $Fe_3O_4$ at the desired location (see Fig. 1). More details on the fabrication of permalloy nanowires by e-beam lithography and their detailed magnetic behavior can be found elsewhere [22].

Figure 2(a) shows the measured magnetization versus field ($M$-$H$) curves of a $Fe_3O_4$ nanoparticle sample $F$#1, exhibiting hysteresis and two prominent jumps in each path. Each sweep shows two main jumps corresponding to a vortex nucleation and annihilation. This is consistent with MUMax [24] micromagnetic simulations [15] using magnetic parameters [25] appropriate for these MNPs. When the magnetic field $H$ is swept back and forth repeatedly, the annihilation or nucleation does not always occur precisely at the same field value, leading to a distribution in measured $H_{sw}$ as shown in the inset histogram of Fig. 2(a). In contrast, another nanoparticle $F$#2 displays a nonzero remanence [see Fig. 2(b)], suggesting a curling mode. Each jump in a sweep occurs at one of two distinct field values, leading to the observation of two disjoint peaks in the switching-field histograms. The presence of two distinct reversal pathways is inferred from the correlation between the nucleation and annihilation field values. Two paths can arise from two slightly different trajectories of the vortex. Another possibility is the vortex chirality in the sense of a
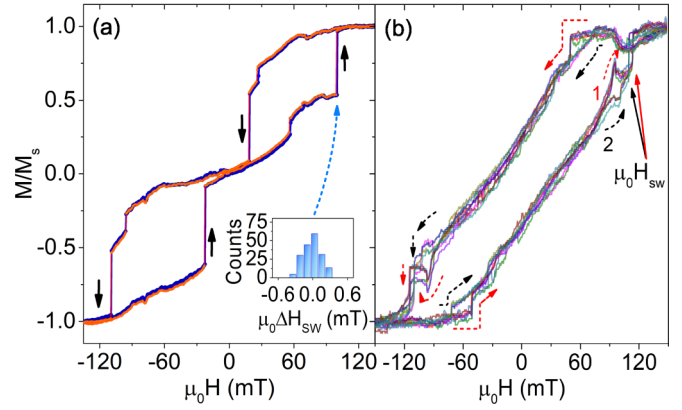
vortex with clockwise or anticlockwise spin order. A defect can possibly lead to an affinity for one chirality vortex over the other leading to a difference in the nucleation and annihilation fields. It may not always be possible to differentiate between parallel pathways, particularly if the switching-field distributions of individual pathways have a width exceeding their separation. In the present study, we observe only one or at most two pathways or MEPs, each displaying a very narrow $H_{sw}$ distribution.

In a magnetic nanostructure, a vortex or a vortex pair is expected to follow an MEP in an energy landscape determined by the external field, the crystalline anisotropy, the exchange energy, the demagnetizing field, and defects. In general, this energy landscape is a $2N_s$-dimensional surface [26–28] due to the $N_s$ spins in the nanoparticle with each having two angular degrees of freedom. The switching-time statistics can provide a way to probe the nature of the MEP(s) at any fixed field close to the threshold $H_{sw}$. Multiple parallel MEPs can arise for a vortex [see Fig. 3(a)], with each path exhibiting different barriers [see Figs. 3(b) and 3(c)]. These 2D surfaces are only schematic diagrams as opposed to the actual complex energy landscape in $2N_s$ dimensions. Along an MEP, the escape rate from an energy minimum depends on the product of the attempt rate, determined by the dynamics near the minimum, and the probability of overcoming the barrier by thermal activation or quantum tunneling.

We define the cumulative distribution function (CDF) for *not switching* during a time $t$ as $P(t)$, as well as the probability density function (PDF) $p(t)$ with $p(t)dt$ being the probability of switching during the time interval $t$ to $t + dt$. These two are related by $P(t) = 1 - \int_0^t p(s)ds$. The PDF provides the histogram of the waiting times before switching at a fixed waiting field $H_w$ close to the switching field $H_{sw}$. For the case of a single barrier, the probability of switching in a time interval $dt$ is $dt/\tau$ with $\tau$ as the mean switching time. With this, one gets $p(t) = \tau^{-1} \exp(-t/\tau)$, and $P(t) = \exp(-t/\tau)$.
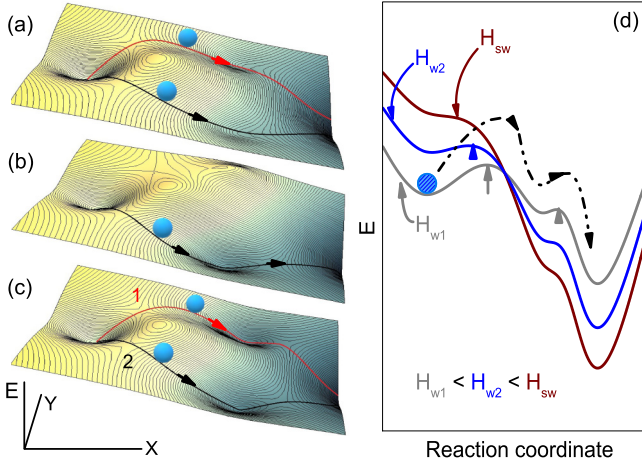
FIG. 3. (a)–(c) show, respectively, the schematic of the free-energy landscape for fields close to the switching field to illustrate two parallel minimum energy paths, two serial barriers in a single path, and two parallel paths with two serial barriers in each. (d) shows the schematic of the energy landscape for two serial barriers at different applied fields close to the switching field $H_{sw}$. This illustrates how the barriers disappear one by one as one tilts the energy landscape by increasing $H$.
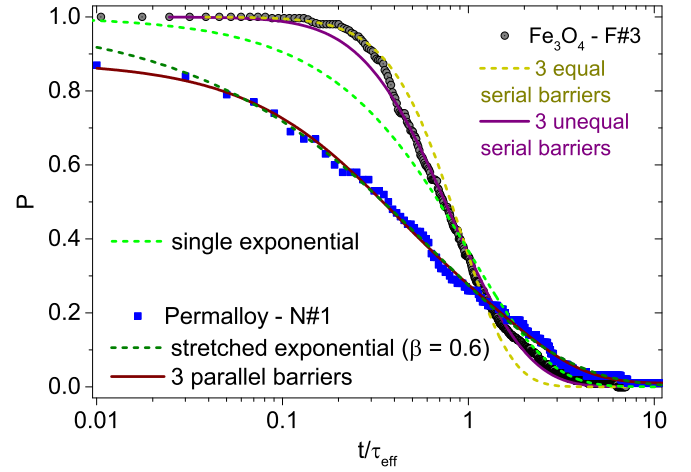


FIG. 4. A comparison of experimental CDF of not switching for an $Fe_3O_4$ nanoparticle at 129.2 mT and that of a permalloy nanowire at 63 mT. The horizontal time axis is in units of respective $\tau_{eff}$. The fits to three equal ($\tau/3 = \tau_{eff} = 25.73$ s) and unequal serial barriers (see Table I) are shown for the nanoparticle data. The fits to the stretched exponential ($\beta = 0.6$ and $\tau = 0.65\tau_{eff} = 3.23$ s) and three parallel barriers (see Table S1 in Supplemental Material [15]) are shown for the nanowire data. The green line shows an exponential with average switching time as $\tau_{eff}$.

The case of $N$ independent parallel paths [see Fig. 3(a)] is a relevant scenario to analyze. Here, the $i$th path has a single barrier, with an associated transition rate $\tau_i^{-1}$. This leads to a CDF,

$$P_{\text{par}}(t) = \sum_{i=1}^{N} w_i e^{-t/\tau_i}. \tag{1}$$

Here, $w_i$ is the probability of selection of the $i$th path with $\sum_i w_i = 1$. The effective mean transition time is then $\tau_{eff} = \sum_i w_i \tau_i$. Many parallel barriers can lead to a behavior close to the stretched-exponential relaxation given by $P_{\text{str}}(t) = \exp[-(t/\tau)^\beta]$ with $\beta < 1$. A precise stretched exponential results from a systematic probability distribution of transition rates [29]. In the case of a statistical ensemble of particles, this could be easily justified but for an isolated particle with only a few parallel paths there is no reason *a priori* to expect the same.

For two barriers in series the overall probability of transition in time $t$ is the convolution of two PDFs: $p_i(t) = \tau_i^{-1} \exp(-t/\tau_i)$ $(i = 1, 2)$, given by $\int_0^t \int_0^{t-t_1} p_1(t_1)p_2(t_2)dt_2 dt_1$. This is deduced by dividing the total time $t$ into $t_1$ and $t_2$ with no transition up to $t_1$ followed by the first barrier crossing in an interval $dt_1$, and then again no transition for a time $t_2$ followed by the second barrier crossing in $dt_2$. For two unequal-transition-rate barriers, i.e., $\tau_1 \neq \tau_2$, this convolution leads to the CDF of not switching as $P_{2u}(t) = (\tau_1 e^{-t/\tau_1} - \tau_2 e^{-t/\tau_2})/(\tau_1 - \tau_2)$. For equal-transition rates, i.e., $\tau_1^{-1} = \tau_2^{-1} = \tau^{-1}$, this becomes $P_{2e}(t) = (1 + \frac{t}{\tau})e^{-t/\tau}$ with the mean switching time as $2\tau$.

Generalizing the two-serial-barrier scenario, the overall probability of a transition across $N$ barriers in series is a convolution of $N$ exponentials: $p_i(t) = \tau_i^{-1} \exp(-t/\tau_i)$ $(i = 1, 2, \ldots, N)$. This gives the CDF of not switching as

$$P_N(t) = 1 - \int_0^t \int_0^{t-t_1} \int_0^{t-t_1-t_2} \cdots \int_0^{t-t_1-t_2\cdots-t_{N-1}}$$
$$\times p_1(t_1)p_2(t_2)p_3(t_3)\cdots p_N(t_N)dt_N \cdots dt_3 dt_2 dt_1. \tag{2}$$

For $N$ barriers, of equal-transition rate $\tau^{-1}$, in series, Eq. (2) leads to

$$P_{Ne}(t) = e^{-Nt/\tau_{eff}} \sum_{k=0}^{N-1} \frac{(Nt/\tau_{eff})^k}{k!}, \tag{3}$$

where $\tau_{eff} = N\tau$ is the overall mean switching time. Note that this expression is the product of $e^{-Nt/\tau_{eff}}$ and the truncated polynomial expansion of $e^{+Nt/\tau_{eff}}$. In the case of $N$ unequal $\tau_i$'s, the CDF works out as

$$P_{Nu}(t) = \sum_i \frac{\tau_i^{N-1}}{f_i(\tau_1, \tau_2, \ldots, \tau_N)} e^{-t/\tau_i}, \tag{4}$$

with $f_i(\tau_1, \tau_2, \ldots, \tau_N) = \prod_{j \neq i}(\tau_i - \tau_j)$. The transition of $P_{Ne}(t)$ from 1 to 0 becomes steeper with increasing $N$ [15] and the corresponding PDF $p(t)$ becomes a more sharply peaked function of width $\propto \tau_{eff}/\sqrt{N}$. The CDF thus has a transition from 1 to 0 over a much narrower time window, as compared to an exponential relaxation. Also, the distribution of $H_{sw}$ is narrower, though the details of its histogram will depend on the dependence of $\tau_i$ on the applied field and its sweep rate. For a single field-dependent barrier, the probability distribution of $H_{sw}$ has been discussed by Kurkijärvi [30].

In order to illustrate the immense difference of behaviors that can be observed in various magnetic micro- or nanostructures, Fig. 4 shows the measured probabilities of not switching $P(t)$ for a permalloy nanowire and a $Fe_3O_4$ nanoparticle. In

units of average switching time $\tau_{eff}$, the permalloy nanowire data spread over more than three time decades. Moreover, they fit to the multiple parallel barrier model or to a stretched exponential [15]. This is similar to the Ni nanowire studied by Wernsdorfer *et al.* [13]. On the other hand, the $Fe_3O_4$ nanoparticle data only have about a decade spread. A similar behavior has been reported in amorphous Co particles with compressed-exponential fits [31].

From micromagnetic simulations [15], it is seen that in a nanomagnet of size below 200 nm a nucleated vortex needs to cross a threshold position in order to annihilate and complete the magnetization reversal. Thus, one can expect the energy landscape to exhibit two relatively deep and well-separated minima that determine the vortex position near nucleation and near annihilation. This will result in a single barrier along the MEP. However, in the presence of defects or even otherwise, the energy landscape may also exhibit other bulges, and dents in which the vortex can get trapped, thus increasing the effective number of barriers. We qualitatively interpret the observed CDF of the $Fe_3O_4$ nanoparticle as due to the presence of multiple barriers along the MEP for magnetization reversal.

In order to have a more quantitative approach, let us consider the switching statistics in the three studied nanoparticles and at various in-plane angles of the magnetic field. In $F$#1 and $F$#3, only one reversal path was seen in the $M$-$H$ loops for every studied angle, temperature, and sweep rate. For $F$#2, we see the early signature of bifurcation (during nucleation) that can be used to select and probe the switching-time statistics in each path. However, here we have actually probed the higher switching-field path, i.e., path-1, where we use no switching until about 1 mT below the path-1 switching field, which is well above the path-2 switching field, as an indicator of path-1. This is possible since the two path's switching-field histograms are well separated. Figure 5 shows the CDF for different waiting-field $H_w$ values near annihilation and nucleation for the three studied $Fe_3O_4$ nanoparticles. These data could not be fitted with a two-serial-barrier model, nor to any parallel barrier model. In contrast, a nice fit is obtained with a three-serial-barrier model for every data set, as shown by the solid lines in Fig. 5. As seen from the reduced $\chi$-square $\chi_r^2$ values (see Table I), the agreement is remarkable.

A systematic evolution of the fitting parameters of the three-serial-barrier model with increasing $H_w$ is presented in Table I. The mean switching time $\tau_{eff}$ decreases rapidly with increasing $H_w$ and two out of the three times, i.e., $\tau_{2,3}$, gradually decrease to zero with increasing $H_w$. This indicates that two of the three serial barriers disappear as the switching field is approached. This aspect is better seen in the histograms, corresponding to the PDF, in Fig. 6 for $F$#3. Remarkably, for the waiting field closest to the thermodynamic switching field, the PDF of a single exponential appears to be the only choice. This is markedly different from the two other histograms in the sense that it does not show a decline down to the smallest waiting times. The disappearance of intermediate barriers when the magnetic field is close to the thermodynamic switching field is consistent with the schematic of Fig. 3(d). When the magnetic field is increased, the whole potential profile is tilted. Some dents will cease to be actual energy minima, thus reducing the number of barriers along the MEP.
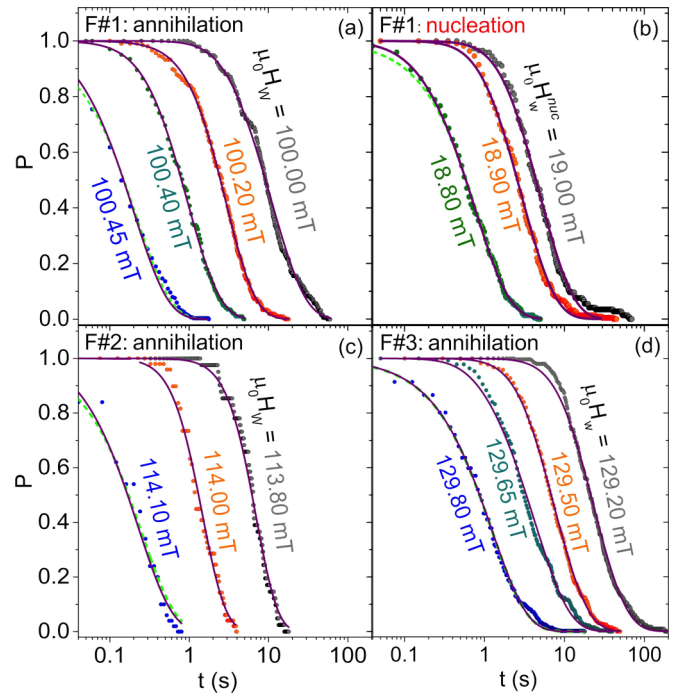


FIG. 5. Experimental CDF of not switching vs time (dots) for $Fe_3O_4$ nanoparticle $F$#1 at $\theta = -45°$, $T = 4.0$ K obtained at waiting fields close to (a) annihilation and (b) nucleation. (c) and (d) show the CDF obtained for $F$#2 at $T = 4.2$ K, $\theta = 0°$ and $F$#3 at $T = 2.0$ K, $\theta = 60°$ respectively. The purple lines are fits to the three unequal barrier models and the green dashed lines are fits to a single exponential.

A comparison of these data has also been made with a compressed exponential and a log-normal distribution [15]. The latter gives a good agreement. A log-normal distribution can indeed be used for describing multiplicative processes [32–34] where a series of barriers is crossed simultaneously rather than one by one.

In conclusion, while the various studied $Fe_3O_4$ particles differ in their detailed $M$-$H$ loop, thus suggesting that the reversals happen through a vortex or through a curling mode, all

TABLE I. Fitting parameters for CDF for not switching for different $H_w$ for $Fe_3O_4$ devices corresponding to Fig. 5. Here, $\tau_{eff}$ is the effective mean switching time. Note that $\tau_{eff}$ decreases rapidly and $\tau_{2,3}$ decreases to zero with increasing field.

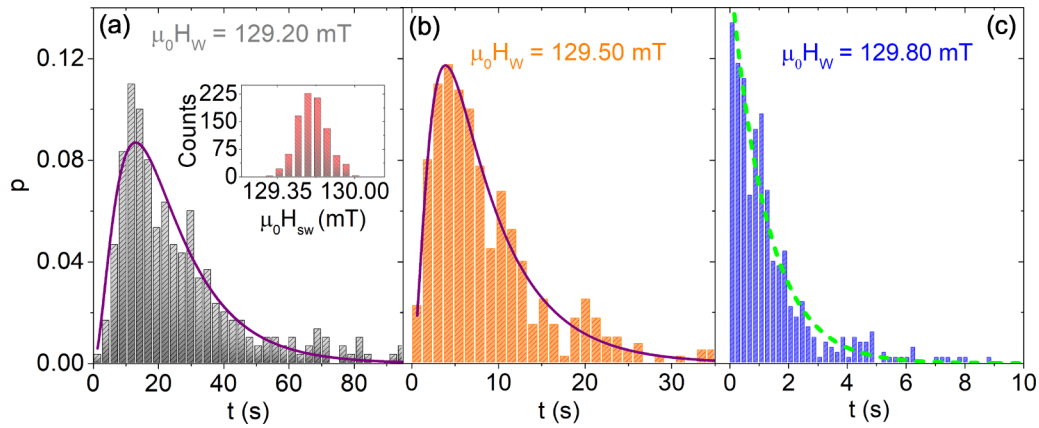| Dev. No. | $\mu_0 H_w$ (mT) | Three unequal serial barriers | | | | |
|---|---|---|---|---|---|---|
| | | $\tau_1$ (s) | $\tau_2$ (s) | $\tau_3$ (s) | $\tau_{eff}$ (s) | $\chi_r^2 \times 10^4$ |
| $F$#1 | 100.00 | 10.79 | 0.82 | 0.82 | 12.43 | 4.5 |
| | 100.20 | 2.32 | 0.81 | 0.00 | 3.13 | 0.7 |
| | 100.40 | 0.89 | 0.17 | 0.00 | 1.06 | 1.2 |
| | 100.45 | 0.20 | 0.01 | 0.00 | 0.21 | 4.7 |
| $F$#3 | 129.20 | 21.56 | 3.00 | 3.00 | 27.56 | 2.1 |
| | 129.50 | 7.06 | 0.91 | 0.91 | 8.88 | 0.8 |
| | 129.65 | 4.24 | 0.19 | 0.19 | 4.62 | 2.6 |
| | 129.80 | 1.25 | 0.00 | 0.00 | 1.25 | 1.3 |

FIG. 6. Waiting-time histograms for $Fe_3O_4$ nanoparticle $F\#3$ at different waiting fields $H_w$, $T = 2.0$ K, and $\theta = 60°$. A large number (~400) of switching data was acquired. The purple line in (a), (b) shows a fit to the PDF corresponding to an unequal barrier model while the green dashed line in (c) shows a fit to an exponential PDF. The inset is a switching-field histogram for this particle with 800 counts obtained at the same temperature, angle, and at a sweep rate of 0.3 mT/s.

of them show strikingly narrow switching-field histograms. At a given applied field close to the switching field, the relaxation to the ground state is best described by a model involving a few barriers in series. The number of barriers required to fit the data reduces as the waiting field is increased, down to one very close to the thermodynamic switching field. For a system with serial barriers, obtaining experimentally the switching-time histograms is much easier, due to a much narrower spread than in a system with parallel barriers. On the same note, such a sharp and definite switching in a non-single-domain particle draws attention towards the applications in decisive switching. The present serial-barrier model can also apply to other multistate systems. In particular, it may help in understanding the role of defects in manipulating the topological magnetic textures such as skyrmion and domain walls in racetrack-type memory devices.

[1] S. S. P. Parkin, M. Hayashi, and L. Thomas, Magnetic domain-wall racetrack memory, Science **320**, 190 (2008).

[2] D. A. Allwood, G. Xiong, C. C. Faulkner, D. Atkinson, D. Petit, and R. P. Cowburn, Magnetic domain-wall logic, Science **309**, 1688 (2005).

[3] X. Zhang, Y. Zhou, K. M. Song, T.-E. Park, J. Xia, M. Ezawa, X. Liu, W. Zhao, G. Zhao, and S. Woo, Skyrmion-electronics: Writing, deleting, reading and processing magnetic skyrmions toward spintronic applications, J. Phys.: Condens. Matter **32**, 143001 (2020).

[4] C. Psaroudaki and C. Panagopoulos, Skyrmion Qubits: A New Class of Quantum Logic Elements Based on Nanoscale Magnetization, Phys. Rev. Lett. **127**, 067201 (2021).

[5] X. Zhang, M. Ezawa, and Y. Zhou, Magnetic skyrmion logic gates: conversion, duplication and merging of skyrmions, Sci. Rep. **5**, 9400 (2015).

[6] A. Jordan, R. Scholz, P. Wust, H. Fahling, and R. Felix, Magnetic fluid hyperthermia (MFH): Cancer treatment with AC magnetic field induced excitation of biocompatible super-paramagnetic nanoparticles, J. Magn. Magn. Mater. **201**, 413 (1999).

[7] E. C. Stoner and E. P. Wohlfarth, A mechanism of magnetic hysteresis in heterogeneous alloys, IEEE Trans. Magn. **27**, 4 (1991); C. Tannous and J. Gieraltowski, The Stoner-Wohlfarth model of ferromagnetism, Eur. J. Phys. **29**, 475 (2008).

[8] M. Jamet, W. Wernsdorfer, C. Thirion, D. Mailly, V. Dupuis, P. Mélinon, and A. Pérez, Magnetic Anisotropy of a Single Cobalt Nanocluster, Phys. Rev. Lett. **86**, 4676 (2001).

[9] L. Néel, Théorie du traînage magnétique des ferromagnétiques en grains fins avec application aux terres cuites, Ann. Geophys. **5**, 99 (1949).

[10] W. F. Brown, Thermal Fluctuations of a Single-Domain Particle, Phys. Rev. **130**, 1677 (1963).

[11] L. Gunther and B. Barbara, Quantum tunneling across a domain-wall junction, Phys. Rev. B **49**, 3926 (1994).

[12] A. Garg, Escape-field distribution for escape from a metastable potential well subject to a steadily increasing bias field, Phys. Rev. B **51**, 15592 (1995).

[13] W. Wernsdorfer, B. Doudin, D. Mailly, K. Hasselbach, A. Benoit, J. Meier, J.-Ph. Ansermet, and B. Barbara, Nucleation of Magnetization Reversal in Individual Nanosized Nickel Wires, Phys. Rev. Lett. **77**, 1873 (1996).

[14] W. Wernsdorfer, E. Bonet Orozco, K. Hasselbach, A. Benoit, B. Barbara, N. Demoncy, A. Loiseau, H. Pascard, and D. Mailly, Experimental Evidence of the Néel-Brown Model of Magnetization Reversal, Phys. Rev. Lett. **78**, 1791 (1997).

[15] See Supplemental Material at http://link.aps.org/supplemental/10.1103/PhysRevB.105.L180410 for micromagnetic simulations, comparison of serial barrier with other scenarios and analysis of permalloy needle data.

[16] M. J. Martínez-Pérez, B. Müller, D. Schwebius, D. Korinski, R. Kleiner, J. Sesé, and D. Koelle, NanoSQUID magnetometry of individual cobalt nanoparticles grown by focused electron beam induced deposition, Supercond. Sci. Technol. **30**, 024003 (2017).

[17] T. Schwarz, R. Wölbing, C. F. Reiche, B. Müller, M. J. Martínez-Pérez, T. Mühl, B. Büchner, R. Kleiner, and D. Koelle, Low-Noise YBa$_2$Cu$_3$O$_7$ Nano-SQUIDs for Performing Magnetization-Reversal Measurements on Magnetic Nanoparticles, Phys. Rev. Appl. **3**, 044011 (2015).

[18] M. J. Martínez-Pérez, J. Pablo-Navarro, B. Müller, R. Kleiner, C. Magén, D. Koelle, J. M. de Teresa, and J. Sesé, NanoSQUID magnetometry on individual as-grown and annealed Co nanowires at variable temperature, Nano Lett. **18**, 7674 (2018).

[19] N. Kumar, T. Fournier, H. Courtois, C. B. Winkelmann, and A. K. Gupta, Reversibility of Superconducting Nb Weak Links Driven by the Proximity Effect in a Quantum Interference Device, Phys. Rev. Lett. **114**, 157003 (2015).

[20] S. Biswas, C. B. Winkelmann, H. Courtois, and A. K. Gupta, Josephson coupling in the dissipative state of a thermally hysteretic micro-SQUID, Phys. Rev. B **98**, 174514 (2018).

[21] S. Biswas, C. B. Winkelmann, H. Courtois, and A. K. Gupta, Elimination of thermal hysteresis with large $V$-$\phi$ transduction in $\mu$-SQUIDs by inductive shun, Phys. Rev. B **101**, 024501 (2020).

[22] S. Paul, G. Kotagiri, R. Ganguly, H. Parashari, H. Courtois, C. B. Winkelmann, and A. K. Gupta, Probing magnetism of individual nano-structures using Nb $\mu$-SQUIDs in hysteresis free mode, J. Magn. Magn. Mater. **503**, 166625 (2020).

[23] A weighted quantity of the precursor salt iron nitrate nonahydrate [Fe(NO$_3$)$_3 \cdot$ 9H$_2$O] from Sigma Aldrich was dissolved in a fixed volume of ethylene glycol (solvent) using a magnetic stirrer. This solution was maintained at 160 °C for about 3 h for the reaction to occur until dark precipitates were obtained. The solution was decanted and the powder was washed several times using ethanol to remove the unreacted salt. Subsequently the powder was allowed to dry in a vacuum furnace maintained at 120 °C.

[24] A. Vansteenkiste, J. Leliaert, M. Dvornik, M. Helsen, F. Garcia-Sanchez, and B. V. Waeyenberge, The design and verification of MuMax3, AIP Adv. **4**, 107133 (2014).

[25] E. Lima, Jr., A. L. Brandl, A. D. Arelaro, and G. F. Goya, Spin disorder and magnetic anisotropy in nanoparticles, J. Appl. Phys. **99**, 083908 (2006).

[26] R. Dittrich, T. Schrefl, D. Suess, W. Scholz, H. Forster, and J. Fidler, A path method for finding energy barriers and minimum energy paths in complex micromagnetic systems, J. Magn. Magn. Mater. **250**, 12 (2002).

[27] C. Serpico, G. Bertotti, M. Aquino, C. Ragusa, P. Ansalone, and I. D. Mayergoyz, Path integral approach to stochastic magnetization dynamics in uniaxial ferromagnetic nanoparticles, IEEE Trans. Magn. **44**, 11 (2008).

[28] P. F. Bessarab, V. M. Uzdin, and H. Jónsson, Method for finding mechanism and activation energy of magnetic transitions, applied to skyrmion and antivortex annihilation, Comput. Phys. Commun. **196**, 335 (2015).

[29] O. Edholm and C. Blomberg, Stretched exponentials and barrier distributions, Chem. Phys. **252**, 221 (2000).

[30] J. Kurkijärvi, Intrinsic fluctuations in a superconducting ring closed with a Josephson junction, Phys. Rev. B **6**, 832 (1972).

[31] W. Wernsdorfer, K. Hasselbach, A. Sulpice, A. Benoit, J.-E. Wegrowe, L. Thomas, B. Barbara, and D. Mailly, Dynamical measurement of domain-wall nucleation and annihilation in individual amorphous Co particles, Phys. Rev. B **53**, 3341 (1996).

[32] W. Shockley, On the statistics of individual variations of productivity in research laboratories, Proc. IRE **45**, 279 (1957).

[33] E. W. Montroll and M. F. Shlesinger, On $1/f$ noise and other distributions with long tail, Proc. Natl. Acad. Sci. USA **79**, 3380 (1982).

[34] A. Amir, Y. Orega, and Y. Imry, On relaxations and aging of various glasses, Proc. Natl. Acad. Sci. USA **109**, 1850 (2012).